Adaptive optics performance model for optical interferometry

D. Mozurkewich,[1] S. R. Restaino,[2] J. T. Armstrong,[2,*] and G. C. Gilbreath[2]

[1]Seabrook Engineering, 9310 Dubarry Avenue, Seabrook, Maryland 20706, USA
[2]U.S. Naval Research Laboratory, 4555 Overlook Avenue SW, Washington, DC 20375, USA

*Corresponding author: tom.armstrong@nrl.navy.mil

Received 12 October 2006; revised 28 February 2007; accepted 2 March 2007;
posted 16 March 2007 (Doc. ID 76022); published 20 June 2007

The optical interferometry community has discussed the possibility of using adaptive optics (AO) on apertures much larger than the atmospheric coherence length in order to increase the sensitivity of an interferometer, although few quantitative models have been investigated. The aim of this paper is to develop an analytic model of an AO-equipped interferometer and to use it to quantify, in relative terms, the gains that may be achieved over an interferometer equipped only with tip–tilt correction. Functional forms are derived for wavefront errors as a function of spatial and temporal coherence scales and flux and applied to the AO and tip–tilt cases. In both cases, the AO and fringe detection systems operate in the same spectral region, with the sharing ratio and subaperture size as adjustable parameters, and with the interferometer beams assumed to be spatially filtered after wavefront correction. It is concluded that the use of AO improves the performance of the interferometer in three ways. First, at the optimal aperture size for a tip–tilt system, the AO system is as much as ~50% more sensitive. Second, the sensitivity of the AO system continues to improve with increasing aperture size. And third, the signal-to-noise ratio of low-visibility fringes in the bright-star limit is significantly improved over the tip–tilt case.

OCIS codes: 010.1080, 010.1330, 110.5100, 120.3180.

1. Introduction

Extending the imaging capabilities of optical interferometry, either to fainter objects or to the low-fringe visibilities that characterize detailed structure, requires larger apertures. Making use of larger apertures depends in turn on adaptive optics (AO) of a higher order than the tip–tilt correction used on current interferometers. In this paper, we model the application of AO to optical interferometry (OI) in order to obtain a quantitative estimate of the improvement in sensitivity that can be achieved in an AO-equipped interferometer over a tip–tilt-equipped interferometer. We have also started an experimental program [1] to evaluate the combination of AO and OI at the Navy Prototype Optical Interferometer (NPOI).

The key results of our modeling are, first, that combining AO and OI produces a significant gain in sensitivity over tip–tilt correction, even at aperture sizes D of ~3 to 4 times the atmospheric coherence length (r_0) where the performance of a tip–tilt system peaks [2] and, second, that the sensitivity of AO-corrected OI continues to improve as the aperture size grows, rather than declining as in the case of tip–tilt correction. The first of these results agrees with the conclusion of Baldwin and Haniff [3] that combining AO and OI should produce a factor of 2 increase in sensitivity for $D \sim 3r_0$, but the second result demonstrates that the benefits of applying AO to OI can be significantly greater. A third result, which follows from the first two, is that low-visibility fringes from bright, resolved stars are also significantly improved by the use of AO.

Optical interferometry is limited by the spatial and temporal dimensions of atmospheric turbulence, characterized by r_0, the coherence length defined by Fried [4] and t_0, the atmospheric coherence time (we

0003-6935/07/204413-10$15.00/0

Report Documentation Page

Form Approved
OMB No. 0704-0188

1. REPORT DATE	2. REPORT TYPE	3. DATES COVERED
2007		**00-00-2007 to 00-00-2007**

4. TITLE AND SUBTITLE	5a. CONTRACT NUMBER
Adaptive optics performance model for optical interferometry	5b. GRANT NUMBER
	5c. PROGRAM ELEMENT NUMBER
6. AUTHOR(S)	5d. PROJECT NUMBER
	5e. TASK NUMBER
	5f. WORK UNIT NUMBER
7. PERFORMING ORGANIZATION NAME(S) AND ADDRESS(ES) **Naval Research Laboratory,4555 Overlook Avenue, SW,Washington,DC,20375**	8. PERFORMING ORGANIZATION REPORT NUMBER
9. SPONSORING/MONITORING AGENCY NAME(S) AND ADDRESS(ES)	10. SPONSOR/MONITOR'S ACRONYM(S)
	11. SPONSOR/MONITOR'S REPORT NUMBER(S)

12. DISTRIBUTION/AVAILABILITY STATEMENT
Approved for public release; distribution unlimited

13. SUPPLEMENTARY NOTES

14. ABSTRACT

15. SUBJECT TERMS

16. SECURITY CLASSIFICATION OF:			17. LIMITATION OF ABSTRACT	18. NUMBER OF PAGES	19a. NAME OF RESPONSIBLE PERSON
a. REPORT **unclassified**	b. ABSTRACT **unclassified**	c. THIS PAGE **unclassified**	**Same as Report (SAR)**	**10**	

adopt the definition advocated by Buscher [5]). Once the collecting aperture or the integration time exceeds a few times r_0 or t_0, the interference fringe signal-to-noise ratio S begins to decrease. AO is subject to the same limitation; we need to correct the wavefront over lengths that scale with r_0 and over times that scale with t_0. Because the number of photons needed for tracking fringes is comparable to the number needed to correct the wavefront, the sensitivity of the two techniques, i.e., the minimum number of photons N per coherence volume $t_0 r_0^2$ needed to reach a given signal-to-noise ratio for wavefront or fringe sensing, should be approximately equal. This is the essence of Baldwin and Haniff's claim that the benefits of combining AO and OI are limited.

However, this argument misses a key point: The number of photons needed to track fringes is gathered from the whole aperture, not just an approximately r_0-sized patch. Thus increasing the overall aperture size decreases the demand for fringe-tracking photons from each subaperture, making more photons available for AO for each subaperture. In a more qualitative vein, the occurrance of a maximum in fringe sensitivity at a modest multiple of r_0 clearly indicates that those photons are not being used in an optimum way. Increasing the aperture increases the number of photons available for tip–tilt sensing but decreases wavefront quality, so some of the photons allocated for tip–tilt should be used for sensing higher-order aberrations instead.

Our AO + OI model, although based in part on numerical simulations of tip–tilt errors, expresses the dependence of sensitivity on such factors as flux, AO servo bandwidth, and AO subaperture size in analytic terms. Although not as accurate as a numerical approach with more error terms, an analytic model favors intuitive understanding. This approach also has the advantage of clearly showing what assumptions we made and where approximations were used. To keep the model reasonably uncoupled from assumptions about the source and instrument, we assume that the interferometer and the AO operate in the same spectral region, with a fraction f of the flux sent to the AO system and the rest passed to the fringe-detection system. Although having the AO and OI work in different spectral regions will affect the absolute sensitivity, it should have no effect on the point of the paper, which is the qualitative behavior of sensitivity as a function of aperture size.

We break the modeling into several pieces. In Section 2, we start by quantifying the dependence on subaperture size, integration time, and servo bandwidth of the wavefront variance for an AO system based on a Shack–Hartman wavefront sensor. We then discuss, in Section 3, optimizing the wavefront by varying subaperture size and integration time. In Section 4, we consider the application of AO to interferometry. Under the assumption that the AO and fringe detection systems share the same wavelength range, we determine how the optimal division of light between the two systems varies with N. We then calculate the resulting overall sensitivity, including the effect of spatially filtering both interferometry beams after wavefront correction. For comparison, in Section 5 we examine the case of an interferometer with only tip–tilt correction. We finish with a discussion in Section 6, including systems in which f or the number of subapertures across the telescope diameter cannot be varied, and a summary in Section 7.

2. Adaptive Optics: Modeling Wavefront Variance

We start by modeling the propagation of a wavefront through an AO system on a single aperture of diameter D, operating with subapertures of diameter A and a servo time constant t_s. We generate a wavefront using a standard Kolmogorov representation of the atmosphere, in which the variance of the phase difference (in radians) between two points separated by B is given by [4]

$$\sigma^2(B) = 6.88(B/r_0)^{5/3}. \quad (1)$$

Our conceptual AO system uses a Shack–Hartman sensor for each subaperture to detect local tilt and to drive a tip–tilt controller for that subaperture. We assume that continuity of the deformable mirror will control differential piston effects between subapertures.

After the AO correction, the wavefront is not perfectly flat. The remaining variations are attributable to three contributions: a residual tilt error within each subaperture, distortion at higher spatial frequencies within each subaperture after tilt and piston terms are removed, and time evolution of the wavefront between measuring the errors and applying the corrections. We will assume that these errors are independent and add their variances. Our decomposition of the errors is similar to the approach taken by Angel [6], although that work is in the high-Strehl-ratio regime.

Our model is not perfect. First, it neglects correlations between the three sources of error. Second, it lacks any treatment of scintillation. We argue that scintillation is unimportant here: Areas in the wavefront that contribute few photons to the AO also contribute few photons to the interferometry. Including the effects of scintillation is important for modeling a high-Strehl-ratio system but not for the low-Strehl-ratio system we describe here. We next describe each of the terms in sequence.

A. Residual Tilt Error

The sensor for each subaperture is a quad cell. Determining how the variance of the position measurement depends on flux entailed generating simulated wavefronts and calculating the resulting images through a subaperture of size A/r_0. For each of 1000 simulations, we calculated the variation dQ/dx of the error signal Q due to an angular error x. This procedure was repeated for a range of values of A/r_0. These simulations give a residual tilt variance σ_Q^2, in radi-

ans, that is well fit over the range $0 < A/r_0 < 5$ by

$$\sigma_Q^2 = \left(\frac{\lambda}{A}\right)^2 \frac{Q_1 + Q_2(A/r_0)^2}{n}, \tag{2}$$

with $Q_1 = 1.39$ and $Q_2 = 0.29$, where n is the number of photons in the integration.

To convert σ_Q into a phase variance, consider a circular aperture of diameter A centered at the origin of the x, y plane. A tilt of θ rad along the x axis produces a delay error across the aperture equal to $x\theta$. The mean delay error is zero. The delay variance is given by

$$\sigma_d^2 = (\theta A)^2 \frac{1}{4\pi} \int\int x^2 \mathrm{d}x\mathrm{d}y = \left(\frac{\theta A}{4}\right)^2, \tag{3}$$

where the area of the integral is bounded by the unit circle. Replacing θ with σ_Q and noting that the phase variance $\sigma_{tt}^2 = (2\pi/\lambda)^2\sigma_d^2$, we find that

$$\sigma_{tt}^2 = \left(\frac{2\pi}{\lambda}\right)^2 \left(\frac{A}{4}\right)^2 \sigma_Q^2, \tag{4}$$

$$= \left(\frac{\pi}{2}\right)^2 \frac{Q_1 + Q_2(A/r_0)^2}{n}. \tag{5}$$

The number of detected photons should be normalized to a standard integration time and aperture. We will use the coherence time and length, t_0 and r_0, for these standards. Using N for the number of photons per coherence volume $t_0 r_0^2$ gives

$$n = N\left(\frac{t}{t_0}\right)\left(\frac{A}{r_0}\right)^2. \tag{6}$$

For our purposes, $t = t_s$, the servo time constant, giving

$$\sigma_{tt}^2 = \left(\frac{\pi^2}{4N}\right)\left(\frac{t_s}{t_0}\right)^{-1}\left[Q_1\left(\frac{A}{r_0}\right)^{-2} + Q_2\right]. \tag{7}$$

B. Higher-Order Distortion

Because the AO takes out the low-spatial-frequency variations, the variance of the higher-order distortions for the entire aperture is the same as the variance for a single subaperture. Noll [7] calculates these partially corrected wavefront variances. For the case in which piston, tip, and tilt are completely removed, the relevant variance is Δ_3 from Noll's Table IV:

$$\sigma_{ho}^2 = \alpha\left(\frac{A}{r_0}\right)^{5/3}, \tag{8}$$

with $\alpha = 0.134$.

C. Wavefront Evolution

The AO system generates a wavefront correction for wavefront errors corresponding to the middle of the integration. By the time this correction is applied, it is out of date by approximately t_s, the servo time constant, and the wavefront has evolved. However, it is only the evolution of the tip–tilt of the subaperture that matters; piston has no effect on the AO, and the higher-order variations are not corrected. All three change the wavefront, but only tip–tilt changes alter the variance.

For the sake of having a closed-form expression, we replace the tip–tilt power spectrum for the subaperture with the power spectrum $\Phi(\nu)$ for the phase difference between two points separated by the subaperture diameter A. This form has the correct total power but somewhat overestimates the high-frequency contribution, a conservative assumption; the exact form falls off as $\nu^{-11/3}$ at high frequencies [8]:

$$\Phi^2(\nu) = p_0 {t_0}^{-5/3} \nu^{-8/3} \qquad \text{for } \nu > \nu_a \tag{9}$$

$$= p_0 {t_0}^{-5/3} {\nu_0}^{-2} \nu^{-2/3} \quad \text{for } \nu < \nu_a, \tag{10}$$

where

$$\nu_a = \frac{d r_0}{A t_0}, \tag{11}$$

the frequency corresponding to spatial scales comparable to A. The constant $d = 0.062$ is derived from Buscher *et al.* [5] while p_0 is $8\pi^2$ times the value in Buscher *et al.*, which converts it to units of radians^2/Hz for a one-sided, rather than two-sided, power spectrum.

The effect of a first-order servo with time constant t_s on the tip–tilt power can be approximated by multiplying the power spectrum by $(\nu t_s)^2$ for frequencies less than $1/t_s$. For $\nu_a t_s < 1$, the power that is not corrected by the angle tracking servo is the integral of this filtered power spectrum and accounts for the time evolution term, given by

$$\sigma_E^2 = \beta\left(\frac{t_s}{t_0}\right)^{5/3} - \gamma\left(\frac{A}{r_0}\right)^{-1/3}\left(\frac{t_s}{t_0}\right)^2, \tag{12}$$

with $\beta = 18p_0/5$ and $\gamma = 18p_0 d^{1/3}/7$.

Finally, we combine the three contributions to the wavefront variance. To simplify the notation, we define $a = A/r_0$, $\tau = t_s/t_0$, $q_1 = \pi^2 Q_1/4$, and $q_2 = \pi^2 Q_2/4$. The values work out to be $q_1 = 3.43$, $q_2 = 0.716$, $\alpha = 0.134$ (as above), $\beta = 0.081$, and $\gamma = 0.023$. Then

$$\sigma^2 = \frac{q_1}{N a^2 \tau} + \frac{q_2}{N\tau} + \alpha a^{5/3} + \beta\tau^{5/3} - \frac{\gamma\tau^2}{a^{1/3}}. \tag{13}$$

3. Minimizing Wavefront Variance

In this section we solve the problem of adjusting τ and a to produce a minimum variance wavefront at a given N, the number of photons per coherence volume. We start with the partial derivatives of Eq. (13):

$$\frac{\partial \sigma^2}{\partial \tau} = -\frac{q_1}{Na^2\tau^2} - \frac{q_2}{N\tau^2} + \frac{5}{3}\,\beta\tau^{2/3} - 2\,\frac{\gamma\tau}{a^{1/3}}, \tag{14}$$

$$\frac{\partial \sigma^2}{\partial a} = -\frac{2q_1}{Na^3\tau} + \frac{5}{3}\,\alpha a^{2/3} + \frac{1}{3}\,\frac{\gamma\tau^2}{a^{4/3}}. \tag{15}$$

Setting these two partials equal to zero produces two equations in three unknowns, i.e., N and the optimal values of a and τ:

$$\frac{q_1}{Na^2} + \frac{q_2}{N} = \frac{5}{3}\,\beta\tau^{8/3} - 2\,\frac{\gamma\tau^3}{a^{1/3}}, \tag{16}$$

$$\frac{q_1}{Na^2} = \frac{5}{6}\,\alpha a^{5/3}\tau + \frac{1}{6}\,\frac{\gamma\tau^3}{a^{1/3}}. \tag{17}$$

These can be solved for $\tau(N)$ and $a(N)$. We first define $\rho = \tau/a$, where τ and a are at their optimal values. We then solve for $N(\rho)$; the algebraic details can be found in Appendix A. We find that

$$N^3 = 6^3\,\frac{{q_2}^7}{{q_1}^4}\,\frac{(5\alpha\rho + \gamma\rho^3)^4}{(10\beta\rho^{8/3} - 5\alpha\rho - 13\gamma\rho^3)^7} \tag{18}$$

$$= \frac{0.499}{\rho^3}\,\frac{(1 + 0.0341\rho^2)^4}{(-1 + 1.205\rho^{5/3} - 0.443\rho^2)^7}. \tag{19}$$

Although we do not have an exact inversion of this equation,

$$\rho = 0.6677N^{-0.333} + 1.114N^{0.0078} \tag{20}$$

gives N to better than 1% for $N < 250$. Figure 1 shows the fit.

The optimal subaperture size and the integration time can be found by inverting Eq. (16) to yield

$$a = \left[\frac{N}{6q_1}(5\alpha\rho + \gamma\rho^3)\right]^{-3/14}, \tag{21}$$

$$= 2.083\left[N(\rho + 0.0341\rho^3)\right]^{-3/14}. \tag{22}$$

From this expression, we determine the normalized servo time constant, τ, from a and the definition of ρ. The optimum subaperture and integration time as a function of N are shown in Fig. 2.

The final step is to calculate the minimum phase variance across a subaperture from Eq. (13) using the optimal values of a and τ. The result is plotted in Fig. 3. It is clear that AO can be useful with only a few

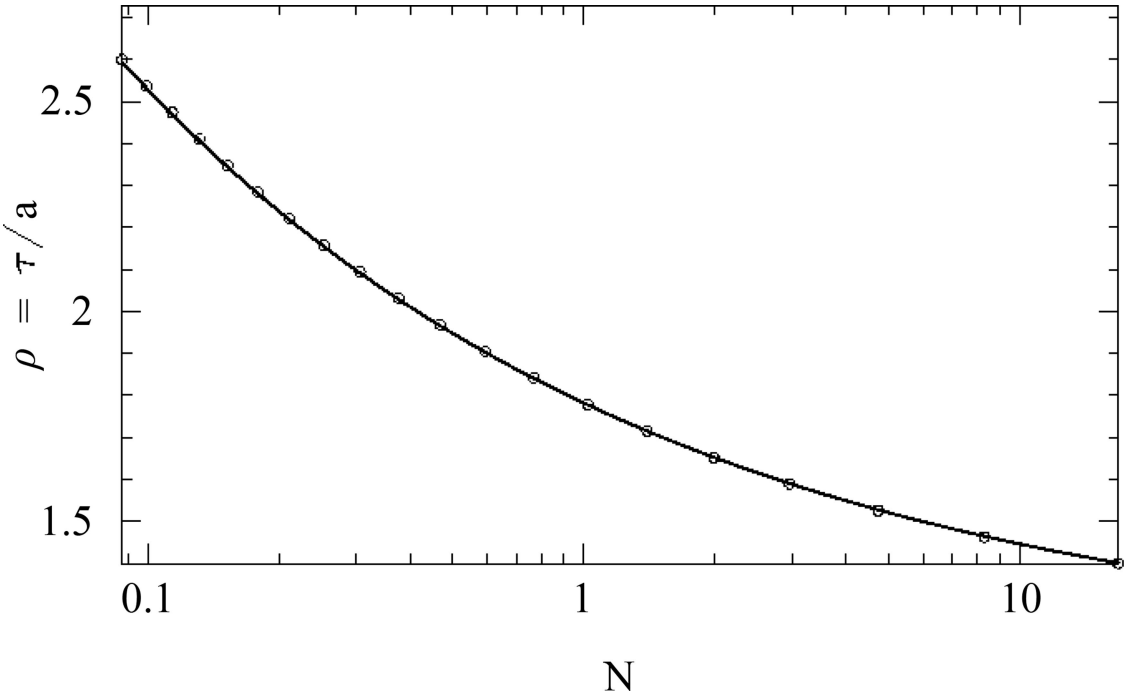

Fig. 1. Variation of $\rho = \tau/a$ as a function of N, the number of photons delivered to the adaptive optics system. The points are the evaluation of Eq. (18). The curve is the approximation of Eq. (20).

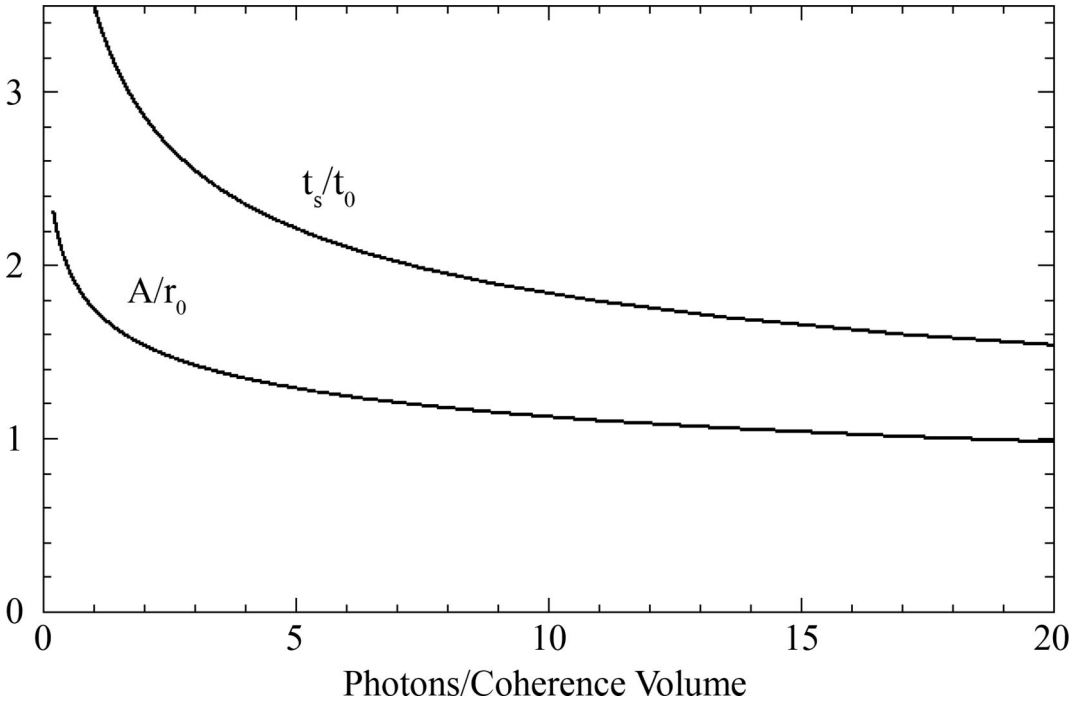

Fig. 2. Optimum values for $a \equiv A/r_0$ and $\tau \equiv t_s/t_0$ as a function of the number of photons per coherence volume N delivered to the adaptive optics system.

detected photons per coherence volume. We show the dependence of the wavefront variance on departures from the optimum values for a and τ in Fig. 4.

To simplify the computations in the next section, we approximate the variance with

$$\sigma^2 = {\sigma_0}^2 + bN^{-c}, \tag{23}$$

$$= 0.0449 + 1.261N^{-0.450}, \tag{24}$$

where the parameters σ_0, b, and c are defined by the first line. This form fits the exact expression to better than 2% for $N < 250$.

4. Interferometry Model

In this section, we apply our wavefront variance results to our model interferometer in order to derive the best value of f, the fraction of incoming light that is sent to the AO system, and to calculate the functional form of the sensitivity of the interferometer.

Our model interferometer has two apertures, each of diameter D, each collecting N photons per coherence volume, and each with perfect spatial filtering. In everything that follows, we will assume that the integration time for the interferometer, t_I, is equal to the atmospheric coherence time t_0. Changing this assumption does nothing but multiply the right-hand side of Eq. (25) by a factor that may depend on the spectrum of the star. This factor has no effect on the functional form of performance versus star brightness and so does not change the main point of this paper.

We will also assume that the fringe-detection system is photon-noise limited, and that it is in the photon-rich regime ($N_I V^2 > 10$, where N_I is the number of photons delivered to the beam combiner). Note that the photon-rich-regime assumption is consistent with the results of the previous section, in which we conclude that AO can be beneficial with only a small number of photons per coherence volume, because the fringe-detection system receives light from several AO subapertures.

The result of the photon-noise-limit and photon-rich-regime assumptions is that the fringe amplitude signal-to-noise ratio $S = (1/\pi)V\sqrt{N_I}$, where the factor $1/\pi$ is the normalization for four-bin fringe sampling. Thus we have

$$S^2 = \frac{2}{\pi^2} V^2 N(1-f)\left(\frac{t_I}{t_0}\right)\left(\frac{\pi D^2}{4{r_0}^2}\right)e^{-\sigma^2}, \tag{25}$$

in which the leading 2 is from the two apertures, and the factor $e^{-\sigma^2}$ reflects the effect of spatial filtering, which converts wavefront irregularities in the two interferometer beams into flux variations. The phase variance in each beam is σ^2, so in the absence of spatial filtering the phase variance between beams would be $2\sigma^2$, which would reduce V^2 in the combined beam, and thus S^2, by a factor of $e^{-2\sigma^2}$. Spatial filtering instead reduces the flux in each beam, and thus the value of S^2, by a factor of only $e^{-\sigma^2}$.

The performance of the AO system is identical to that derived in the previous section except that the number of photons per coherence volume N is replaced with fN. Equation (23) becomes

$$\sigma^2 = {\sigma_0}^2 + \frac{b}{(fN)^c}, \tag{26}$$

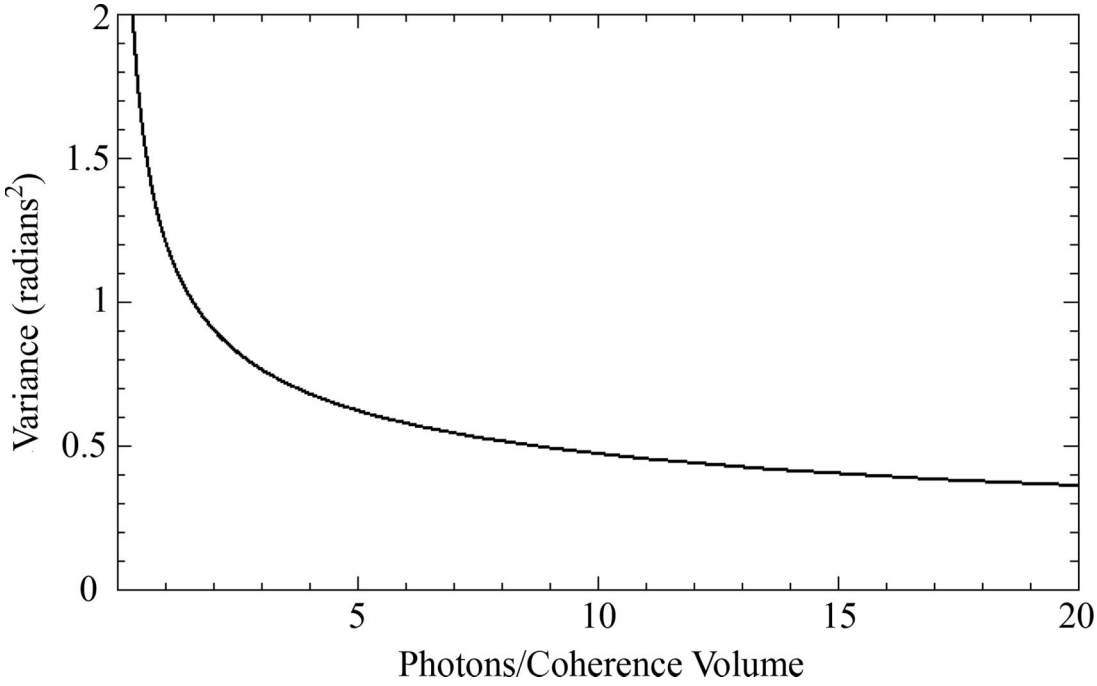

Fig. 3. Phase variance σ^2 across a subaperture as a function of the number of photons per coherence volume N delivered to the adaptive optics sensor for the case in which a and τ are optimized.

so

$$\frac{\mathrm{d}\sigma^2}{\mathrm{d}f} = -\frac{bc}{N^c f^{c+1}}. \tag{27}$$

Maximizing S^2 with respect to f (and assuming the star is unresolved so $V = 1$) yields

$$\frac{\mathrm{d}S^2}{\mathrm{d}f} = -\frac{N}{2\pi}\left(\frac{t_I}{t_0}\right)\left(\frac{D}{r_0}\right)^2 e^{-\sigma^2} - \frac{N}{2\pi}(1-f)\left(\frac{t_I}{t_0}\right)\left(\frac{D}{r_0}\right)^2 e^{-\sigma^2}\frac{\mathrm{d}\sigma^2}{\mathrm{d}f}, \tag{28}$$

$$= 0, \tag{29}$$

which leads to

$$\frac{N^c}{bc} = \frac{1-f}{f^{c+1}}. \tag{30}$$

The optimal fraction f is plotted versus N in Fig. 5. Once again, an exact inversion is lacking, but

$$f = 0.448 - 0.202\log(N) + 0.0177\log^2(N) + 0.00341\log^3(N) \tag{31}$$

is accurate to better than 1% over the relevant range of N.

We are finally in a position to evaluate the sensitivity of an AO-equipped OI as a function of aperture size. Start by returning to Eq. (25) with $t_I = t_0$ and note that σ^2 depends on fN [Eq. (26)], and f depends only on N [Eq. (31)]. Thus S/D depends only on N. We assume a minimum value of $S = 5$ for fringe tracking, calculate S/D, then calculate the value of D needed to achieve our assumed value of S.

The results of this procedure are plotted in Fig. 6, but before discussing these results, we will calculate the sensitivity of OI in some comparison cases—the most important being that of tip–tilt correction only—using the same assumptions as in the AO case.

5. Optical Interferometry with Tip–Tilt Only

A system with only tip–tilt correction is the most important comparison case since most current interferometers operate in this mode. In this case, the fringe tracking signal-to-noise ratio is still governed by Eq. (25), but now D/r_0 is replaced by a. Again taking $t_I = t_0$, we have

$$S^2 = \frac{N}{2\pi}(1-f)a^2 e^{-\sigma^2}. \tag{32}$$

Since there is no optimization for subaperture size in this case, we have to examine the behavior of σ^2 by returning to Eq. (13) and replacing N with fN. Maximizing S^2 with respect to f and τ now gives

$$\frac{\partial S^2}{\partial \tau} = -\frac{N}{2\pi}(1-f)a^2 e^{-\sigma^2}\frac{\partial \sigma^2}{\partial \tau}, \tag{33}$$

$$= 0,$$

and

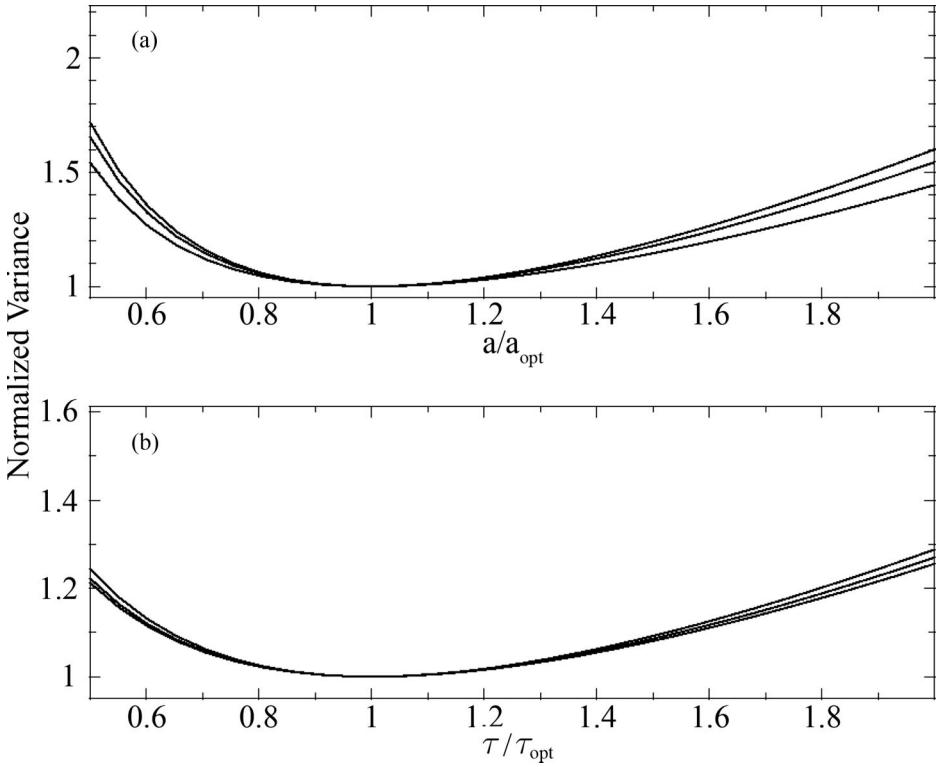

Fig. 4. Phase variance across a subaperture normalized to the variance at the optimal values of a and τ. (a) Normalized variance is plotted as a function of a, the subaperture size in units of r_0, normalized to its optimal value, a_{opt}. The curves, from upper to lower, are calculated for $N = 100$, 10, and 1. (b) Normalized variance is plotted as a function of τ, the AO servo time constant in units of t_0, normalized to its optimal value, τ_{opt}. The curves, from upper to lower, are calculated for $N = 1$, 10, and 100.

$$\frac{\partial S^2}{\partial f} = -\frac{N}{2\pi}\, a^2 e^{-\sigma^2} - \frac{N}{2\pi}(1-f)a^2 e^{-\sigma^2}\,\frac{\partial \sigma^2}{\partial f},$$

$$= 0, \tag{34}$$

where

$$\frac{\partial \sigma^2}{\partial \tau} = -\frac{q_1}{fNa^2\tau^2} - \frac{q_2}{fN\tau^2} + \frac{5}{3}\,\beta\tau^{2/3} - 2\,\frac{\gamma\tau}{a^{1/3}}, \tag{35}$$

$$\frac{\partial \sigma^2}{\partial f} = -\frac{q_1}{f^2Na^2\tau} - \frac{q_2}{f^2N\tau}. \tag{36}$$

Equation (33) reduces to $\partial\sigma^2/\partial\tau = 0$ and can be rearranged to give

$$fN = \frac{q_1 + q_2a^2}{a^2\tau}\left(\frac{5}{3}\,\beta\tau^{5/3} - \frac{2\gamma\tau^2}{a^{1/3}}\right)^{-1}, \tag{37}$$

while combining Eqs. (34), (33), and (35) gives

$$\frac{1}{f} = 1 + \left(\frac{5}{3}\,\beta\tau^{5/3} - \frac{2\gamma\tau^2}{a^{1/3}}\right)^{-1}. \tag{38}$$

We solved this set of equations iteratively for $N(a)$, the number of photons per coherence volume needed to attain the target value of S for a fixed value of a. First, for the given value of a, we guess a value of τ and use Eqs. (37) and (38) to calculate f and N. We use these values in Eq. (32) to find S. We then adjust the value of τ and repeat the process until we obtain the desired value of S. As with the AO case, the results are plotted in Fig. 6.

6. Discussion

Figure 6 shows the photons per coherence volume needed to obtain a signal-to-noise ratio $S = 5$ with an optical interferometer for both the adaptive optics and tip–tilt cases. Two important points should be made.

The first point is that the sensitivity for the tip–tilt case has a peak; for larger apertures, sensitivity actually decreases. Our calculations give $D/r_0 = 3.9$ for the aperture size at peak sensitivity. This result is not new; the literature cites values in the range of 3 to $5r_0$ for the optimal aperture size [2,9].

The second point to be made is that the sensitivity of an AO-endowed system does not peak at some value of D/r_0 but continues to improve as the aperture size increases. This behavior may seem surprising at first, but it can be explained by considering that a larger aperture can devote a larger fraction of its photons to wavefront correction while continuing to gather the total number of photons needed for fringe detection. The fact that sensitivity continues to

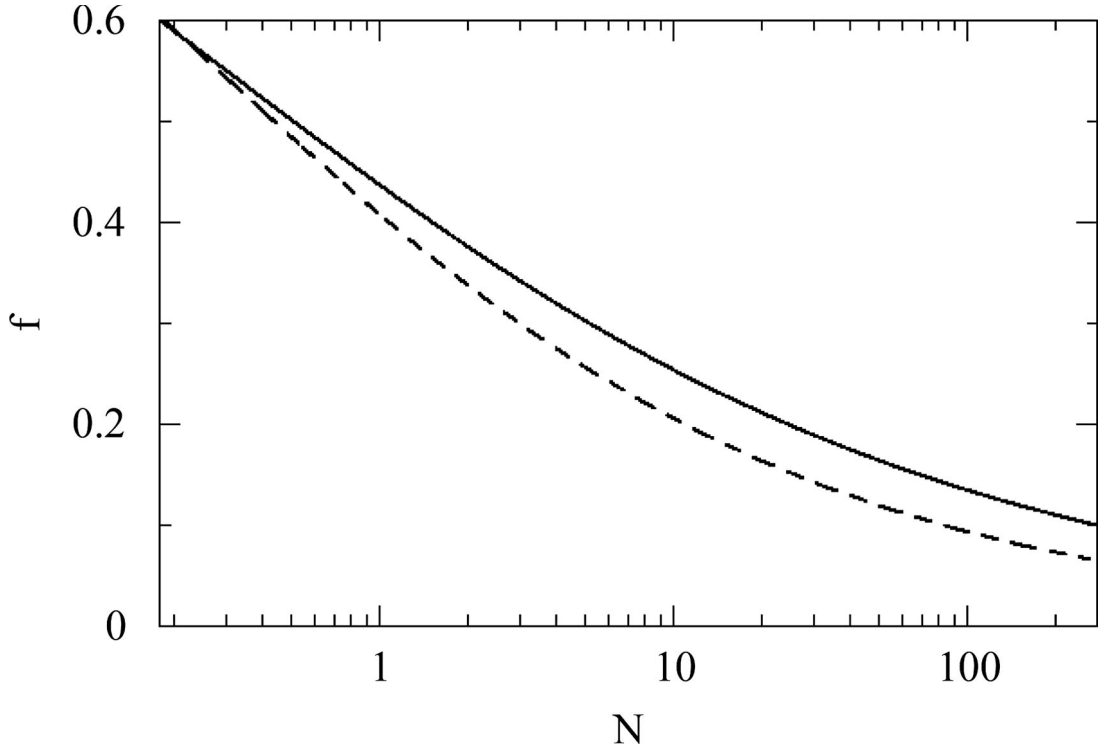

Fig. 5. The fraction of light to send to the adaptive optics system that optimizes the interferometric signal-to-noise ratio as a function of the number of photons per coherence volume presented to the whole system (full curve). For comparison, we plot the same quantity for the tip–tilt case with $D/r_0 = 3.9$, the value for maximum sensivity (dashed curve).

increase with aperture size is important for the design of future interferometers.

Note also that the AO-equipped system is up to 50% more sensitive than the tip–tilt system at the optimal tip–tilt aperture size. Consider a tip–tilt system with the optimal aperture diameter, so that the sensitivity does not vary with a small change in aperture, or equivalently with a small change in the number of detected photons. This lack of dependence of the sensitivity on photon rate implies

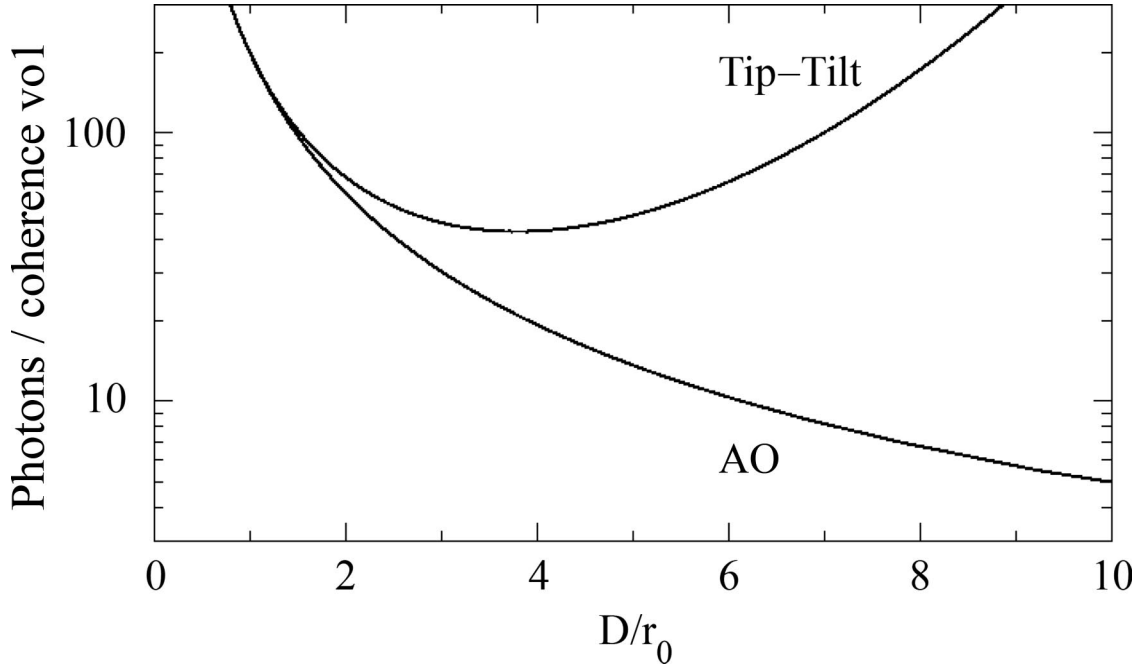

Fig. 6. Photons per coherence volume needed to obtain a fixed signal-to-noise ratio with an optical interferometer, as a function of aperture size, for an adaptive-optics equipped interferometer and for an interferometer with tip–tilt correction only.

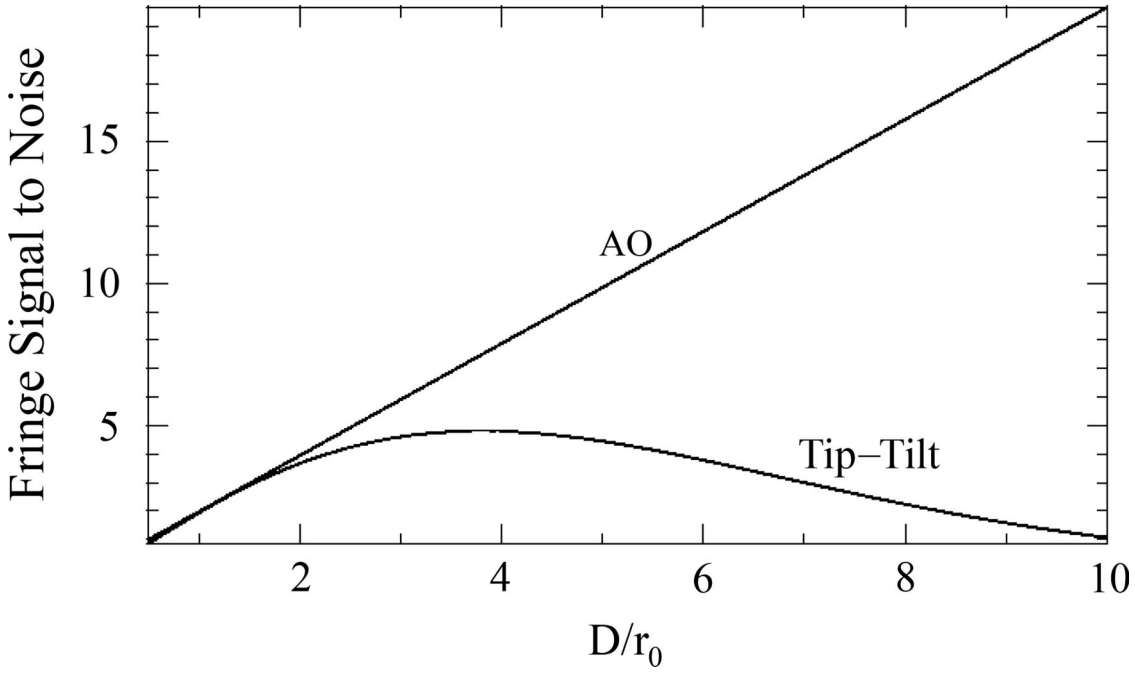

Fig. 7. Signal-to-noise ratio at $V = 1$ as a function of aperture size in the bright-star limit.

that we are not using those photons in an optimal way.

In fact, looking at the contributions to the wavefront variance bears that conclusion out. The tip–tilt error, the only contribution to the variance that depends on the number of photons, is only approximately one third as large as the contribution from higher-order aberrations at low flux ($N \approx 4$) and signal-to-noise ratio ($S \approx 1$), and is smaller still at higher flux levels. We should expect that using more photons to estimate higher-order aberrations, reducing $\sigma_{ho}{}^2$ at the expense of increasing $\sigma_{tt}{}^2$, should improve system performance.

The advantages of an AO-equipped interferometer do not depend critically on the ability to adjust f or a to match conditions. For instance, if f remains fixed at 0.2, roughly the optimal value for faint sources, the sensitivity is within a few percent of the optimal AO result. If the AO system has as few as four subapertures across the telescope diameter, the sensitivity at the faint limit is within ≈10% of the fully adjustable system.

Our discussion has centered so far on the question of the faintest source that can be observed with an interferometer in the fully adjustable AO and tip–tilt cases. However, for stars that are bright enough for either system, it is still advantageous to use AO. The benefit comes in the improved signal-to-noise ratio, which leads directly to more accurate visibility measurements. Highly accurate visibilities are important for precise angular diameter measurements and are critical for limb-darkening and surface structure observations.

To make the comparison for this limit, we examine the performance of the two systems at a fixed value of N. As before, the starting point is Eq. (25):

$$S^2 = \frac{NV^2}{2\pi}(1-f)\left(\frac{D}{r_0}\right)^2 e^{-\sigma^2}. \tag{39}$$

For the tip–tilt case, the choice of N determines σ^2. We follow the same procedure as in the faint-star limit, using Eqs. (37) and (38) to find an equation for $N(a, \tau)$. We then invert this equation to find τ for fixed values of N and a, and use Eq. (39) to determine S. For the AO case, we determine f as before from Eq. (31). Again using the fact that f and σ^2 can be expressed as functions of N alone, we calculate S directly from Eq. (39). Figure 7 shows the signal-to-noise ratio of the two systems at fringe visibility $V = 1$.

To evaluate the sensitivity of the two systems to low visibilities, we inverted Eq. (39) to find $V(S, N)$. The overall picture is very similar to the faint-star limit: The optimal aperture size for the tip–tilt case is $\sim 4r_0$, the AO-equipped system outperforms the tip–tilt system, and S continues to increase with D/r_0 for the AO case.

7. Summary

This paper presents an analytic model for assessing the performance of an optical interferometer fitted with adaptive optics (AO), and uses the model to compare the performance of an AO-equipped interferometer with one using only tip–tilt correction.

The AO-equipped interferometer performs better for all aperture sizes larger than approximately $0.5r_0$, where r_0 is the coherence length of the atmosphere. The best performance of the tip–tilt corrected system is at aperture sizes near $4r_0$, but even for those ap-

erture sizes, the AO-equipped system is superior by a factor of approximately 2. In addition, the AO-equipped system continues to gain in sensitivity with increasing aperture size, asymptotically approaching a maximum in performance. At aperture sizes of $10r_0$, the AO-equipped system is ~10 times as sensitive as the tip–tilt system's sensitivity at $\sim 4r_0$, where it performs best. For bright stars, those within reach of both systems, the AO-equipped system has significant advantages in fringe signal-to-noise ratio and in the smallest detectable visibility.

These results are preliminary; clearly the model can be improved by including parameterization based on both detailed numerical analysis and experimental values. Nevertheless, it is clear that adding AO to an OI can significantly improve its limiting magnitude, as well as its ability to measure visibilities with high precision.

Appendix A. Derivation of Optimization of τ and a

To find the integration time τ and subaperture size a that minimize the wavefront variance σ^2, we start with Eqs. (16) and (17):

$$\frac{q_1}{Na^2} + \frac{q_2}{N} = \frac{5}{3}\beta\tau^{8/3} - \frac{2\gamma\tau^3}{a^{1/3}}, \tag{A1}$$

$$\frac{q_1}{Na^2} = \frac{5}{6}\alpha a^{5/3}\tau + \frac{\gamma\tau^3}{6a^{1/3}}, \tag{A2}$$

which can be solved for $\tau(N)$ and $a(N)$. First eliminate q_1 from Eq. (A1):

$$\frac{q_2}{N} + \frac{5}{6}\alpha a^{5/3}\tau + \frac{13}{6}\frac{\gamma\tau^3}{a^{1/3}} = \frac{5}{3}\beta\tau^{8/3}. \tag{A3}$$

Set $\rho = \tau/a$ and eliminate τ from Eqs. (A2) and (A3):

$$\frac{q_1}{N} = a^{14/3}\left(\frac{5}{6}\alpha\rho + \frac{1}{6}\gamma\rho^3\right), \tag{A4}$$

$$\frac{q_2}{N} = a^{8/3}\left(\frac{5}{3}\beta\rho^{8/3} - \frac{5}{6}\alpha\rho - \frac{13}{6}\gamma\rho^3\right). \tag{A5}$$

Now eliminate a:

$$\left(\frac{q_1}{N}\right)^{3/14}\left(\frac{q_2}{N}\right)^{-3/8} = \left(\frac{5}{6}\alpha\rho + \frac{1}{6}\gamma\rho^3\right)^{3/14}\left(\frac{5}{3}\beta\rho^{8/3} - \frac{5}{6}\alpha\rho - \frac{13}{6}\gamma\rho^3\right)^{-3/8}, \tag{A6}$$

and solve for N:

$$N^{9/56} = \frac{{q_2}^{3/8}}{{q_1}^{3/14}}\left(\frac{5}{6}\alpha\rho + \frac{1}{6}\gamma\rho^3\right)^{3/14}\left(\frac{5}{3}\beta\rho^{8/3} - \frac{5}{6}\alpha\rho - \frac{13}{6}\gamma\rho^3\right)^{-3/8} \tag{A7}$$

$$N^3 = 6^3\frac{{q_2}^7}{{q_1}^4}\frac{(5\alpha\rho + \gamma\rho^3)^4}{(10\beta\rho^{5/3} - 5\alpha\rho - 13\gamma\rho^3)^7}. \tag{A8}$$

We thank the anonymous reviewers for comments that helped clarify this paper. This research was supported by the the Office of Naval Research.

References

1. S. R. Restaino, J. Andrews, J. T. Armstrong, T. Martinez, C. Wilcox, and D. Payne, "Navy prototype optical interferometer upgrade with light-weight telescopes and adaptive optics: A status update," *Proceedings of 2006 AMOS Technical Conference* (2006), pp. 105–111.
2. D. F. Buscher, "Getting the most out of C.O.A.S.T.," Ph.D. dissertation (Cambridge University, 1988).
3. J. E. Baldwin and C. A. Haniff, "The application of interferometry to optical astronomical imaging," Philos. Trans. R. Soc. London Ser. A **360,** 969–986 (2002).
4. D. L. Fried, "Optical resolution through a randomly inhomogeneous medium for very long and very short exposures," J. Opt. Soc. Am. **56,** 1372–1379 (1966).
5. D. F. Buscher, J. T. Armstrong, C. A. Hummel, A. Quirrenbach, D. Mozurkewich, K. J. Johnston, C. S. Denison, M. M. Colavita, and M. Shao, "Interferometric seeing measurements on Mount Wilson: Power spectra and outer scales," Appl. Opt. **34,** 1081–1096 (1995).
6. J. R. P. Angel, "Ground-based imaging of extrasolar planets using adaptive optics," Nature **368,** 203–207 (1994).
7. R. J. Noll, "Zernike polynomials and atmospheric turbulence," J. Opt. Soc. Am. **66,** 207–211 (1976).
8. C. B. Hogge and R. R. Butts, "Frequency spectra for the geometric representation of wavefront distortions due to atmospheric turbulence," IEEE Trans. Antennas Propag. **24,** 144–154 (1976).
9. F. Roddier, "The effects of atmospheric turbulence in optical astronomy," Prog. Opt. **XIX,** 281–376 (1981).